



Aalborg Universitet

AALBORG UNIVERSITY
DENMARK

Using computational fluid dynamics to describe H₂S mass transfer across the water–air interface in sewers

Teuber , Katharina; Broecker, Tabea; Bentzen, Thomas Ruby; Stephan, Dietmar; Nützmänn, Gunnar; Hinkelmann, Reinhard

Published in:
Water Science and Technology

DOI (link to publication from Publisher):
[10.2166/wst.2019.193](https://doi.org/10.2166/wst.2019.193)

Creative Commons License
CC BY-NC 4.0

Publication date:
2019

Document Version
Accepted author manuscript, peer reviewed version

[Link to publication from Aalborg University](#)

Citation for published version (APA):

Teuber , K., Broecker, T., Bentzen, T. R., Stephan, D., Nützmänn, G., & Hinkelmann, R. (2019). Using computational fluid dynamics to describe H₂S mass transfer across the water–air interface in sewers. *Water Science and Technology*, 79(10), 1934–1946. <https://doi.org/10.2166/wst.2019.193>

General rights

Copyright and moral rights for the publications made accessible in the public portal are retained by the authors and/or other copyright owners and it is a condition of accessing publications that users recognise and abide by the legal requirements associated with these rights.

- ? Users may download and print one copy of any publication from the public portal for the purpose of private study or research.
- ? You may not further distribute the material or use it for any profit-making activity or commercial gain
- ? You may freely distribute the URL identifying the publication in the public portal ?

Take down policy

If you believe that this document breaches copyright please contact us at vbn@aub.aau.dk providing details, and we will remove access to the work immediately and investigate your claim.

1 Using CFD to describe H₂S mass transfer across the
2 water-air interface in sewers

3 Katharina Teuber (corresponding author)^a

4 Tabea Broecker^a

5 Thomas Ruby Bentzen^b

6 Dietmar Stephan^c

7 Gunnar Nützmann^d

8 Reinhard Hinkelmann^a

9 ^aChair of Water Resources Management and Modeling of Hydrosystems, Technische
10 Universität Berlin, Berlin, Germany

11 ^bDepartment of Civil Engineering, Aalborg University, Aalborg SV, Denmark

12 ^cChair of Building Materials and Construction Chemistry, Technische Universität Berlin,
13 Berlin, Germany

14 ^dLeibniz-Institute of Freshwater Ecology and Inland Fisheries, Berlin, Germany and Humboldt-
15 University of Berlin, Geography Department, Berlin, Germany

16 E-Mail: katharina.teuber@uwi.tu-berlin.de

17 Abstract

18 For the past 70 years, researchers have dealt with the investigation of odour in sewer systems
19 caused by hydrogen sulphide formations and the development of approaches to describe it. The
20 state-of-the-art models are one-dimensional. At the same time, flow and transport phenomena
21 in sewers can be three-dimensional, for example the air flow velocities in circular pipes or flow
22 velocities of water and air in the reach of drop structures. Within the past years, increasing
23 computational capabilities enabled the development of more complex models. This paper uses
24 a three-dimensional two-phase Computational Fluid Dynamics model to describe mass transfer
25 phenomena between the two phases: water and air. The solver has been extended to be capable
26 to account for temperature dependency, the influence of pH value and a conversion to describe
27 simulated air phase concentrations as partial pressure. Its capabilities are being explored in
28 different application examples and its advantages compared to existing models are
29 demonstrated in a highly complex three-dimensional test case. The resulting interH2SFoam
30 solver is a significant step in the direction of describing and analysing H₂S emissions in sewers.

31

32 Keywords: H₂S emissions, numerical simulation, Computational Fluid Dynamics (CFD),
33 OpenFOAM

34 Introduction

35 Wastewater in sewers undergoes a lot of physical and biochemical processes. One important
36 factor is the formation of hydrogen sulphide (H_2S), which can cause health risks for sewer
37 workers. The tendency of more complex and longer sewer networks can lead to longer retention
38 times, which enhance the emission of H_2S . Climate change at the same time causes higher
39 temperatures in the wastewater, which increases emission rates.

40 In the past 70 years extensive research has been performed to increase the knowledge on H_2S
41 formations and to develop approaches, which describe the development of odour in sewers (e.g.
42 Gilchrist 1953, Thistlethwayte 1972). The state-of-the-art models, which have been developed
43 within the last 20 years, are horizontal one-dimensional. These are the SeweX model from
44 Australia (Rootsey and Yuan 2010, Rootsey et al. 2012) and the WATS model from Denmark
45 (Hvitved-Jacobsen et al. 2013). Both are not public domain.

46 An overview of existing model approaches has been given in Carrera et al. (2016) and the need
47 for further research has been highlighted.

48 To begin with, the mass transfer approach of the existing models is based on the so-called two-
49 film theory, which uses different assumptions. The WATS model additionally uses different
50 approaches to account for turbulent H_2S transfer rates across the water surface in various
51 applications. These different approaches are empirical or theoretical connections between
52 oxygen and H_2S transfer on the one hand and empirical models linking H_2S emissions to flow
53 properties in the pipe on the other hand (Carrera et al. 2016).

54 Wang et al. (2018) highlight the shortcomings of the two-film theory. It cannot account for
55 local changes of the flow regime or variations of fluid properties. Furthermore, the theory is
56 based on a constant liquid film that can change in real-life conditions due to flow instabilities.
57 The most limiting factor however is assumed to be the one-dimensionality of the approach.
58 More advanced approaches, the penetration theory and the surface renewal theory, can account
59 for the variability of the flux over time but do not account for local variations, the change of
60 fluid properties or flow regimes (Wang et al. 2018). This has already led to wide applications
61 of CFD models for mass transfer applications in the chemical industry (Wang et al. 2018).

62 Carrera et al (2016) identified the models' lack to describe mass transfer processes across the
63 water surface, the current approaches of which were considered to be simplified, especially
64 when considering hydraulic structures such as gravity sewers, junctions and water falls. Recent
65 research on water falls or drop structures in sewer systems led to improved formulations to
66 account for the effect of local turbulence (Matias et al. 2017), but these approaches are still
67 empirical equations which are fed into the model.

68 This short overview leads to the question whether a three-dimensional simulation model could
69 help in increasing the process understanding, especially when analysing complex and turbulent
70 flows in a sewer. Another benefit could be the in-depth analysis and design optimization in
71 hotspots of H_2S emissions.

72 In order to address this question, a volume of fluid (VOF) approach as it is implemented in
73 OpenFOAM's solver interFoam has been chosen to describe the two-phase flow of water and
74 air. This solver has already been used for a number of demanding hydraulic applications (e.g.

75 Thorenz and Strybny 2012, Bayón et al. 2015) and enables a stable, robust and accurate
76 description of complex flow phenomena.

77 The VOF method is often used to describe mass transfer processes in CFD applications (Wang
78 et al 2018). Therefore, Haroun et al. (2010a, 2010b) have developed an approach to describe
79 mass transfer processes across the interface between two fluids using the Henry coefficient for
80 the VOF method. This approach has been implemented in OpenFOAM's solver interFoam by
81 Nieves-Remacha et al. (2015), Yang et al. (2017) and Severin (2017), resulting in a solver
82 which will be called interHarounFoam in the following.

83 A short outline of the driving biochemical processes leading to H₂S formation shall be given to
84 highlight important factors. When anaerobic conditions occur in the wastewater, sulphate-
85 reducing bacteria, which reside in the biofilms of sewer walls can reduce sulphate to sulphide
86 (Sharma et al., 2008). From the biofilm, sulphide is then diffused into the wastewater as H₂S.
87 In the water, equilibrium conditions depending on the pH value and temperature determine
88 which amounts of sulphide are present as H₂S and as bisulphide ion (HS⁻), together they are
89 described as total dissolved sulphide. The air-water equilibrium, which can be described by the
90 Henry coefficient for a volatile compound such as H₂S, can cause emissions of H₂S from the
91 water into the air phase. The rate of the transfer process is influenced by factors such as the
92 flow velocities within the different phases, the pH value, temperature and the concentration of
93 oxygen and nitrate. The Henry coefficient describes the relative amount of a volatile compound
94 in the gas phase as a function of its relative occurrence in the water phase under equilibrium
95 conditions and at constant temperature. The temperature dependency of Henry's law can be
96 described by different equations, for example by the van't Hoff equation. The concentration of
97 H₂S in the air phase defines the intensity of odour (Hvitved-Jacobsen et al., 2013).

98 As this overview of the relevant processes shows, a sole consideration of the Henry coefficient
99 when describing H₂S emissions is not sufficient. Therefore, relevant extensions have been made
100 to the solver, resulting in a new, specialized solver, interH2SFoam. This solver is able to
101 account for the temperature dependency of the Henry coefficient. Further extensions enable the
102 user to describe the equilibrium between HS⁻ and pH value in the water phase and to compute
103 the partial pressure of H₂S_g in the air phase in ppm in order to gain a better comparability
104 between simulations and measured values. The assessment of turbulent flow effects on mass
105 transfer will be subject to future research.

106 In the following, after an introduction on the methods used, the capabilities of the
107 interH2SFoam solver are explored in three simple application examples of vertical one-
108 dimensional flow. Then, mass transfer in a rectangular pipe is simulated. In a final example, the
109 new solver is applied to a highly complex sewer geometry.

110 Methods

111 Numerical model

112 OpenFOAM version 2.4.0 has been used for the work presented in this paper. Additionally, a
113 supplementary library called swak4Foam has been used to generate customized function objects
114 to calculate the equilibrium conditions between H₂S and HS⁻ as well as the partial pressure in
115 the air phase. This approach makes the use of this function optional for the user. Depending on
116 the framework of the model, the user can then decide whether these functions are needed or
117 not. The temperature dependency on the Henry coefficient of H₂S has been directly
118 implemented in the solver and makes a definition of the temperature as an input parameter
119 mandatory.

120 Hydrodynamic simulations

121 The mass transfer solvers are based on the two-phase flow solver interFoam which is based on
122 a VOF approach that considers both phases as one fluid with changing fluid properties. One set
123 of Navier-Stokes equations is solved. The volume fraction of a phase is stored as an additional
124 variable and the phases are distinguished by an additional transport equation. The equations are
125 defined as follows (Rusche 2002):

126 Mass conservation equation:

$$\nabla \cdot \vec{U} = 0 \quad (1)$$

127 Momentum conservation equation:

$$\frac{\partial \rho \vec{U}}{\partial t} + \nabla \cdot (\rho \vec{U} \vec{U}) = -\nabla p_{rgh} + \nabla \cdot (\mu \nabla \vec{U}) + (\nabla \vec{U}) \nabla \mu - \vec{g} \cdot \vec{x} \nabla \rho \quad (2)$$

128 Where p_{rgh} is the static pressure minus hydrostatic pressure:

$$p_{rgh} = p - \rho g h \quad (3)$$

129 Volume of Fluid equation:

$$\frac{\partial \alpha}{\partial t} + \nabla \cdot (\alpha \vec{U}) + \nabla \cdot ((1 - \alpha) \vec{U}_r \alpha) = 0 \quad (4)$$

130 with the following parameters:

$$\rho = \alpha \rho_{aq} + \rho_g (1 - \alpha) \quad (5)$$

$$\mu = \alpha \mu_{aq} + \mu_g (1 - \alpha) \quad (6)$$

$$\mu_i = \mu_{i,phys} + \mu_{i,turb} \text{ with } i = aq, g \quad (7)$$

131 where \vec{U} is the velocity field [m/s]; ρ is the density [kg/m³]; t is time [s]; p is the pressure [Pa];
132 μ is the dynamic viscosity [Ns/m²]; \vec{g} is the acceleration vector due to gravity [m/s²]; \vec{x} is a
133 spatial position vector [m]; α is a volume fraction or indicator function [-]; \vec{U}_r is the relative
134 velocity between the phases [m/s]; the subscripts aq and g denote the fluids water (aq - aqueous)
135 and air (g - gas). For the dynamic viscosity μ , the physical viscosity μ_{phys} and the turbulent
136 viscosity μ_{turb} are considered (see Equation 7).

137 The indicator function α is defined as:

$$\alpha = \begin{cases} 1 & \text{fluid aq} \\ 0 < \alpha < 1 & \text{transistional region} \\ 0 & \text{fluid g} \end{cases} \quad (8)$$

138

139 The water surface is defined as the area where $\alpha = 0.5$.

140 A turbulence model based on the Reynolds averaged Navier-Stokes equations (Standard k- ϵ) is
141 applied to consider the turbulent part and the near-wall turbulence is modelled by so-called wall
142 functions. More advanced turbulence models, such as Large Eddy Simulations (LES) or Direct
143 Numerical Simulations (DNS), would offer the opportunity of resolving small-scale velocity
144 variations but would come with the price of a highly increased computation time. As we expect
145 that the application of more advanced turbulence effects would not change the insights on the
146 equilibrium conditions of the mass transfer simulations addressed in this publication, a RANS
147 turbulence model has been considered to be sufficient as well as the best way to save
148 computational resources. Even with the Standard k- ϵ turbulence model, the computation time
149 of 10 seconds simulation for the complex sewer geometry amounted to 12 hours on 80 parallel
150 processors using the high performance computing (HPC) clusters of TU Berlin.

151 The accuracy of the hydrodynamic simulations has been assessed in Teuber et al. (in press).

152 *Transport simulations*

153 In general, the transport of a passive tracer with a concentration c is examined with an
154 advection-diffusion equation that can be implemented into the interFoam solver (see Equation
155 9). The physical diffusivity D_{phys} as well as the turbulent Schmidt number Sc_{turb} , which defines
156 the turbulent diffusivity coefficient D_{turb} , then have to be defined by the user (Equation 10).

157 Advection-diffusion equation:

$$\frac{\partial c}{\partial t} + \nabla \cdot (\vec{U}c) = \nabla \cdot (D_{phys} + D_{turb})\nabla c \quad (9)$$

158 with

$$D_{turb} = \frac{\mu_{turb}/\rho}{Sc_{turb}} \quad (10)$$

159

160 *Mass transfer*

161 Mass transfer has been simulated using the approach defined by Haroun et al. (2010a, 2010b)
162 as it has been implemented by Nieves-Remacha et al. (2015) and Severin (2017). The approach
163 is based on the interFoam solver and considers one additional transport equation for both phases
164 as outlined in Equations 9 and 10.

$$\frac{\partial c}{\partial t} + \nabla \cdot (\vec{U}c) = \nabla \cdot ((D_{phys} + D_{turb})\nabla c + \phi) \quad (11)$$

165

166 A concentration flux expression at the interface results in the following:

$$\phi = -(D_{phys} + D_{turb}) \left(\frac{c(1 - He)}{\alpha + He(1 - \alpha)} \right) \nabla \alpha \quad (12)$$

167

168 In order to distinguish the species transport between the two phases, Henry's law must be
169 fulfilled and the concentration flux must be consistent:

$$He = \frac{c_{aq}}{c_g} \quad (13)$$

$$(D_{phys,aq} + D_{turb,aq}) \nabla c_{aq} = (D_{phys,g} + D_{turb,g}) \nabla c_g \quad (14)$$

170 The concentrations and diffusion coefficients are considered as single-phase properties
171 depending on the phase fraction value α :

$$c = \alpha c_{aq} + c_g (1 - \alpha) \quad (15)$$

$$D_{phys} = \left(\frac{D_{phys,aq} D_{phys,g}}{\alpha D_{phys,aq} + (1 - \alpha) D_{phys,g}} \right) \quad (16)$$

172 The diffusion coefficients for D_{aq} and D_g are defined by the user. Note that these coefficients
173 are temperature dependent which has to be taken into account when defining the values.

174 **Henry coefficient**

175 The Henry coefficient, also known as Henry constant, is a temperature dependent variable
176 which is reported in many different forms in literature and is often expressed in different units.

177 In this paper, three different definitions of the Henry coefficient are relevant for the derivation
178 and comparison with analytical solutions. Sander (2015) lists values of Henry coefficients in
179 the unit [mol/(m³Pa)] and defines this Henry coefficient as H^{cp} . For the implementation in the
180 interHarounFoam solver, the dimensionless Henry coefficient H^{cc} is relevant (see Equation 13):

$$H^{cc} = He = \frac{c_{aq}}{c_g} \quad (17)$$

181 Where the Henry coefficient is expressed as the ratio between the concentration in the aqueous
182 phase c_{aq} and the concentration in the gas phase c_g .

183 H^{cp} can be converted to H^{cc} using the ideal gas law:

$$H^{cc} = H^{cp} \cdot R \cdot T \quad (18)$$

184 Where R is the universal gas constant $8.314 \frac{kg \cdot m^2}{s^2 \cdot mol \cdot K}$ and T is the temperature [K].

185 For H₂S, the Henry coefficient at standard temperature (25 °C) results in:

$$H_{H_2S}^{cc} = 10^{-3} \frac{mol \cdot s^2}{m^2 \cdot kg} \cdot 8.314 \frac{kg \cdot m^2}{s^2 \cdot mol \cdot K} \cdot 298.15 K = 2.479 \quad (19)$$

186

187 **Extensions**

188 *Temperature dependency of Henry coefficient*

189 The Henry coefficient depends on the overall temperature in the domain. Therefore, the
190 temperature dependency has been added in a way that the solver takes one global temperature
191 value as an input parameter.

192 The temperature dependent Henry coefficient is computed using the van't Hoff equation
193 following Sander (2015):

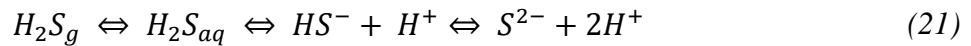
$$H^{cp}(T) = H^{cp} \exp\left(C \left(\frac{1}{T} - \frac{1}{T^\theta}\right)\right) \quad (20)$$

194 Here, C is a temperature coefficient, which depends on the enthalpy of dissolution and is
195 defined as 2100 K (Sander 2015), T^θ is the standard temperature 298.15 K corresponding to
196 25°C.

197 *Equilibrium conditions*

198 The equilibrium conditions are implemented following Hvitved-Jacobsen et al. (2013). The aim
199 is to describe the water-phase concentration of H₂S depending on the amount of total dissolved
200 sulphide and the pH value since those values are usually measured in field investigations.

201 The dissociation of H₂S is generally expressed by the following equilibrium:



202 The equilibrium between H₂S in the gas phase (H₂S_g) and H₂S in the water phase (H₂S_{aq}) is
203 described by the Henry coefficient. In the water phase, an equilibrium between hydrogen
204 sulphide H₂S_{aq} and bisulphide ion (HS⁻) exists, where the total amount of both is described as
205 total dissolved sulphide.

206 Only H₂S_{aq} can be transferred across the air-water interface, not the ionized form HS⁻, however,
207 usually the concentration of total dissolved sulphide and the pH value are measured. Therefore
208 it is useful to derive a way to calculate the concentration of c_{H₂S_{aq}} when c_S and pH are given.

209 The equilibrium depends on the equilibrium constant K_{a1} (also known as acid dissociation
210 constant):

$$K_{a1} = \frac{c_{H^+} c_{HS^-}}{c_{H_2S_{aq}}} \quad (22)$$

211 The dissociation can also be described using the negative logarithm of K_{a1}, pK_{a1} (pK_{a1} = -
212 logK_{a1}), resulting in the Henderson-Hasselbalch equation:

$$\log_{10} \frac{c_{H_2S_{aq}}}{c_{HS^-}} = pK_{a1} - pH \quad (23)$$

213 For a temperature of 20°C the equilibrium constant is pK_{a1} = 7.0. Between the ionized form
214 HS⁻ and the sulphide ion another equilibrium exists in the water phase:



$$K_{a2} = \frac{c_{H^+} c_{S^{2-}}}{c_{HS^-}} \quad (25)$$

215 The value of $pK_{a2} = 14.0$ indicates that measurable amounts of the sulphide ion S^{2-} only exist
 216 at a value above a pH of about 12. Therefore, only the equilibrium value of K_{a1} is important for
 217 wastewater and has been implemented for the interHarounFoam solver in OpenFOAM using
 218 the utilities `funkySetFields` (for initial conditions) and `funkySetBoundaryFields` (as boundary
 219 conditions) from `swak4Foam`.

220 The step-by-step reformulation based on Hvitved-Jacobsen et al. (2013) of the equations which
 221 results in the equation implemented in OpenFOAM is shown in the following, beginning with
 222 the Henderson-Hasselbalch equation:

$$\log_{10} \frac{c_{H_2S_{aq}}}{c_{HS^-}} = pKa_1 - pH \quad (26)$$

223 Solving the log-function and using the expression $c_S = c_{HS^-} + c_{H_2S_{aq}}$ for the total dissolved
 224 sulphide:

$$10^{pKa_1 - pH} = \frac{c_{H_2S_{aq}}}{c_{HS^-}} = \frac{c_{H_2S_{aq}}}{c_S - c_{H_2S_{aq}}} \quad (27)$$

225 Rearranging leads to the mass concentration $\gamma_{H_2S_{aq}}$ in $[kg/m^3]$:

$$\gamma_{H_2S_{aq}} = \frac{c_S \cdot 10^{pKa_1 - pH}}{1 + 10^{pKa_1 - pH}} \quad (28)$$

226 This can be converted into a molar concentration $c_{H_2S_{aq}}$ $[mol/m^3]$ by dividing through the
 227 atomic weight M_S (0.032 kg/mol) of sulphur (S):

$$c_{H_2S_{aq}} = \frac{\gamma_{H_2S_{aq}}}{M_S} = \frac{\gamma_{H_2S_{aq}}}{0.032 \frac{kg}{mol}} \quad (29)$$

228 Thus, the resulting equation implemented in OpenFOAM is:

$$c_{H_2S_{aq}} = \frac{c_S \cdot 10^{pKa - pH}}{1 + 10^{pKa - pH}} \quad (30)$$

229 Note that the equilibrium constants K_{a1} and K_{a2} are temperature dependent (Yongsiri et al.
 230 2004), which is not considered in the current version of the code. The value of K_{a1} is a user-
 231 defined variable and the temperature dependency of the equilibrium constant has to be
 232 accounted for by defining the corresponding K_{a1} value for the temperature analysed.

233 *Calculation of partial pressure of H_2S_g in ppm*

234 The partial pressure of H_2S_g is being computed using a function object in `swak4Foam`.

235 The input value in OpenFOAM is a tracer $c_{H_2S_{aq}}$ in $[mol/m^3]$, requiring a unit conversion:

$$c \left[\frac{mol}{l} \right] = 1 \frac{mol}{l} = \frac{c_{H_2S_{aq}}}{1000} = \frac{1000 \frac{mol}{m^3}}{1000} \quad (31)$$

236 The conversion from ppm to atm is:

$$10^{-6} atm = 1 ppm \quad (32)$$

237 According to Hvitved-Jacobsen et al. (2013), the partial pressure of a trace quantity in the air
 238 phase can be expressed by multiplying the molar concentration with the molar volume:

$$p_{H_2Sg}[atm] = c_{H_2Saq} \left[\frac{mol}{l} \right] \cdot 22.4 \frac{l}{mol} \quad (33)$$

239 Together, this leads to the following equation for conversion:

$$p_{H_2Sg}[ppm] = 10^6 \frac{c_{H_2Saq} \left[\frac{mol}{m^3} \right]}{1000} \cdot 22.4 \frac{l}{mol} \quad (34)$$

240 This conversion is only valid for the gas phase concentration, therefore the expression is
241 multiplied with $(1-\alpha)$ in order to keep the conversion constraint to the air phase.

242

243 Case studies

244 In the following, three different cases will be used to explore the possibilities of the existing
245 solver, to validate the new features added to the solver and to show the importance of the model
246 compared to the existing model approaches. For all simulations, at a temperature of 25°C,
247 physical diffusivities for H₂S in water of $2.2 \cdot 10^{-9} \text{ m}^2/\text{s}$ and in air of $1.74 \cdot 10^{-5} \text{ m}^2/\text{s}$ are chosen.

248 The first setup is a quasi-one-dimensional cubic tank with the measures 1m x 1m x 1m bounded
249 by upper, lower and sidewalls with no-slip conditions. The tank is partially filled with water
250 (water depth $d = 0.5 \text{ m}$). Both fluids water and air are at rest. As an initial condition, an H₂S
251 concentration of $c_{H_2Saq} = 1 \text{ mol}/\text{m}^3$ in the water phase is given, the concentration in the air phase
252 is $c_{H_2Sg} = 0 \text{ mol}/\text{m}^3$. The domain is discretized with 100 cells in y-direction, which is the vertical
253 dimension of the domain, and 10 cells in x- and z-direction. At the bottom wall, a concentration
254 source is assumed, using a fixed value boundary condition of $1 \text{ mol}/\text{m}^3$. The top wall as well as
255 the sidewalls are defined with zeroGradient conditions. This setup is used to illustrate the
256 solver's capabilities in a simple setup. In a first example, mass transfer, as it can be described
257 with the existing interHarounFoam solver, is shown in a vertical one-dimensional case. Then,
258 the extensions leading to the interH2SFoam solver are demonstrated in different examples using
259 this first setup.

260 In a second setup, mass transfer in a rectangular duct is analysed using two well-documented
261 examples of water-air pipe flow as they have been described by Bentzen et al. 2016 (test cases
262 no. 7 and 21). The investigated pipe has a length of 15.0m, a height of 0.26m and a width of
263 0.3m with two different water depths and slopes. The air phase is only accelerated by the
264 movement of the water surface. Bentzen et al (2016) measured resulting velocity profiles in
265 detail using Laser Doppler Anemometry (LDA) velocity measurements. The flow
266 characteristics of the two test cases analysed are listed in Table 1. The setup is a relatively
267 simple three-dimensional setup of a pipe. It illustrates the applicability of the model to regular
268 pipes. The computational domain consists of 307,970 cells. The inlet has been divided in two
269 parts: one for the water phase and one for the air phase. For the water phase, a fixed discharge
270 has been defined, and the phase fraction value α has been defined to be $\alpha = 1$. The pressure
271 boundary condition has been defined as null Neumann condition. For the air phase, a fixed
272 pressure has been defined and the phase fraction value has been set to $\alpha = 0$. The velocity has
273 been defined using a null Neumann condition. At the outlet, a free outflow has been assumed.
274 A fixed pressure has been defined and the remaining boundary conditions were defined as null
275 Neumann conditions. At the walls, no-slip conditions were applied. Hydrodynamic simulations
276 (without mass transfer) were run for 200s, until quasi steady state conditions were reached,
277 afterwards a concentration $c_{H_2Saq} = 1 \text{ mol}/\text{m}^3$ has been defined for the water at the inlet,

278 assuming contaminated water flowing into the domain. The upper fluid then has a concentration
279 of $c_{\text{H}_2\text{Sg}} = 0 \text{ mol/m}^3$ at the inlet, all remaining boundaries were defined with null Neumann
280 conditions.

281 *Table 1. Mass transfer in rectangular channel: flow properties of analysed test cases.*

Test no.	Duct slope (%)	Water depth (cm)	U_{aq} (m/s)	U_{g} (m/s)	Reynolds number Re_{aq}	Reynolds number Re_{g}
7	0.57	3.15	0.77	0.226	72,300	5,400
21	1.34	4.00	1.37	0.336	175,300	7,900

282

283 The third setup describes a complex sewer geometry with an overall length of 93.3m, a width
284 ranging from 6.0m to 7.5m and a sewer height between 4.3m and 5.3m. The setup is shown in
285 Figure 6. This geometry has been simulated in OpenFOAM and compared to experimental
286 results from a 1:20 scale model by Bayón et al (2015) and Teuber et al. (in press). The setup
287 describes a highly three-dimensional pipe diversion, including bends and geometry changes as
288 well as a hydraulic jump. The computational mesh consists of 3,029,223 cells. The setup of
289 boundary conditions is similar to the rectangular pipe of Bentzen et al. (2016). The
290 hydrodynamic model has been simulated for 200s, until steady-state conditions were reached.
291 Then, a concentration $c_{\text{H}_2\text{Saq}} = 1 \text{ mol/m}^3$ has been defined for the water phase and the
292 simulations using the interH2SFoam solver have been carried out for a simulation time of 10s.
293 A temperature of 25°C is assumed.

294 The results of the numerical simulations are presented in the following Section.

295

296 Results and discussion

297 Saturation of H₂S in a tank

298 Mass transfer modelling

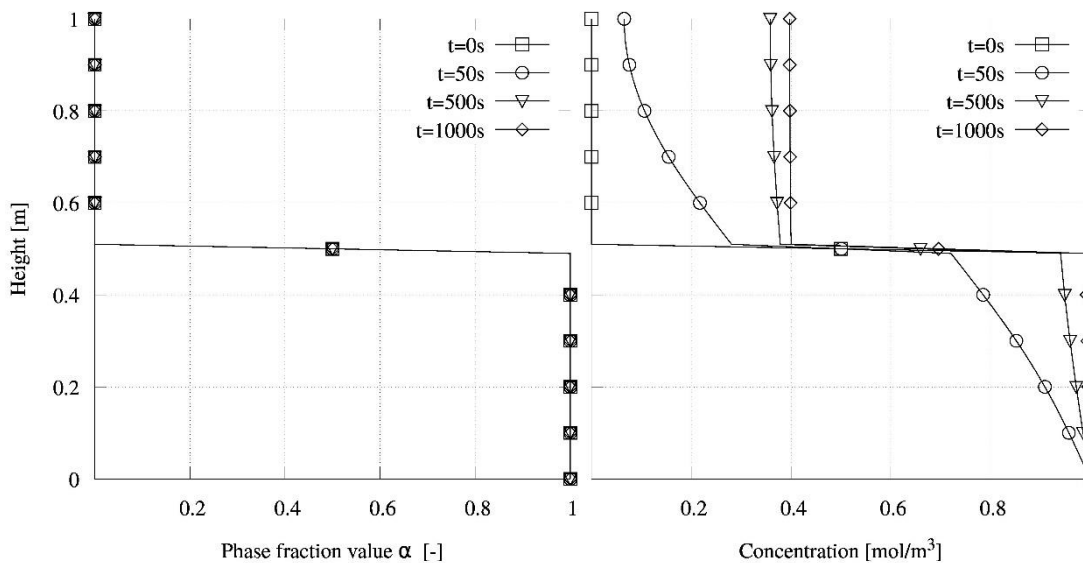
299 In our first test case, we present the application of the model to a vertical one-dimensional
 300 problem. It illustrates the advantage of the new model in describing vertical concentration
 301 profiles in contrast to the existing horizontal one-dimensional approaches. The simplicity of the
 302 test case enables a first illustration of the model's capabilities. The simulation has been carried
 303 out assuming normal temperature (25°C).

304 Figure 1 shows the presence of the two phases within the domain ($\alpha = 1$: water, $\alpha = 0$: air) and
 305 the development of the concentration profile over time. After $t = 50$ s, a decrease of the overall
 306 concentration in the water phase can be observed. This is due to the concentration jump at the
 307 interface, which has to be fulfilled by the solver. This concentration jump occurs in the first
 308 second due to a direct flux of concentration across the interface. After several seconds, the
 309 concentration in the water phase is re-established by the source term at the bottom and after $t =$
 310 1000 s, a steady-state has developed and a constant concentration profile is achieved. The
 311 concentration in the water phase is then equal to the source term concentration and the air phase
 312 concentration is defined by the Henry coefficient. A detailed validation of the flux under
 313 transient conditions has been performed by Haroun et al. (2010a).

314 The concentration profile illustrates that the resulting air phase concentration is $c_{H_2Sg} = 0.4034$
 315 mol/m^3 , which is the expected concentration in the air phase when applying Henry's law for
 316 H₂S:

$$c_{H_2Sg} = \frac{c_{H_2Saq}}{H_{H_2S}^{cc}} = \frac{1 \frac{\text{mol}}{\text{m}^3}}{2.479} = 0.4034 \frac{\text{mol}}{\text{m}^3} \quad (35)$$

317



318

319 Figure 1. H₂S saturation in a tank (left: phase fraction value, right: concentration profiles along the vertical axis over time).

320 *Temperature dependency*

321 In this test case, we will analytically analyse the temperature dependency of the Henry
 322 coefficient, which has been implemented. The application example is based on example 4.2 in
 323 Hvitved-Jacobsen et al. (2013). The Henry coefficient at a temperature of 15°C is being
 324 calculated.

325 In this case, a temperature of 288.15 K has been chosen. The resulting Henry coefficient can be
 326 determined as follows (following Equations 18-20):

$$H^{cc}(T) = H^{cp} \exp\left(C \left(\frac{1}{T} - \frac{1}{T^\theta}\right)\right) R T \quad (36)$$

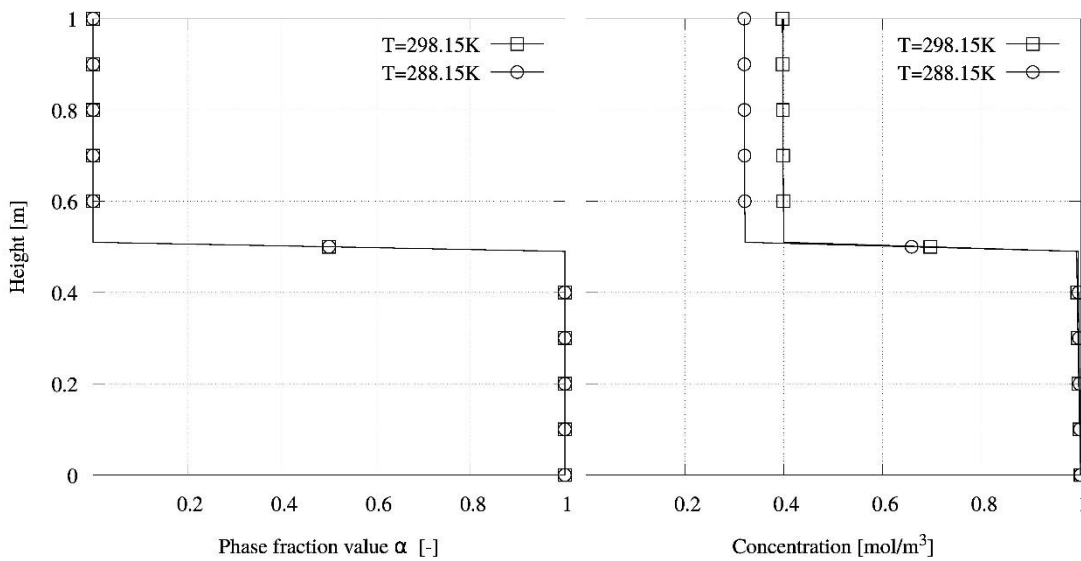
$$H^{cc}(288.15) = 0.001 \cdot \exp\left(2200 \left(\frac{1}{288.15} - \frac{1}{298.15}\right)\right) \cdot 8.314 \cdot 288.15 \quad (37)$$

$$H^{cc}(288.15) = 3.083 \quad (38)$$

327 Resulting in the following expected gas-phase concentration $c_{H_2S,g} = 0.324 \text{ mol/m}^3$:

$$c_{H_2S,g}(288.15) = \frac{1}{3.083} = 0.324 \quad (39)$$

328 Figure 2 shows the resulting concentration in the domain after $t = 1000s$. The result agrees well
 329 with the expected concentration. The implemented temperature dependency can therefore be
 330 considered as accurate.



331
 332 *Figure 2. H₂S saturation in a tank for different temperatures (298.15K (cp. Figure 1, right) and 288.15K) (left: phase fraction*
 333 *value, right: concentration profiles along the vertical axis).*

334

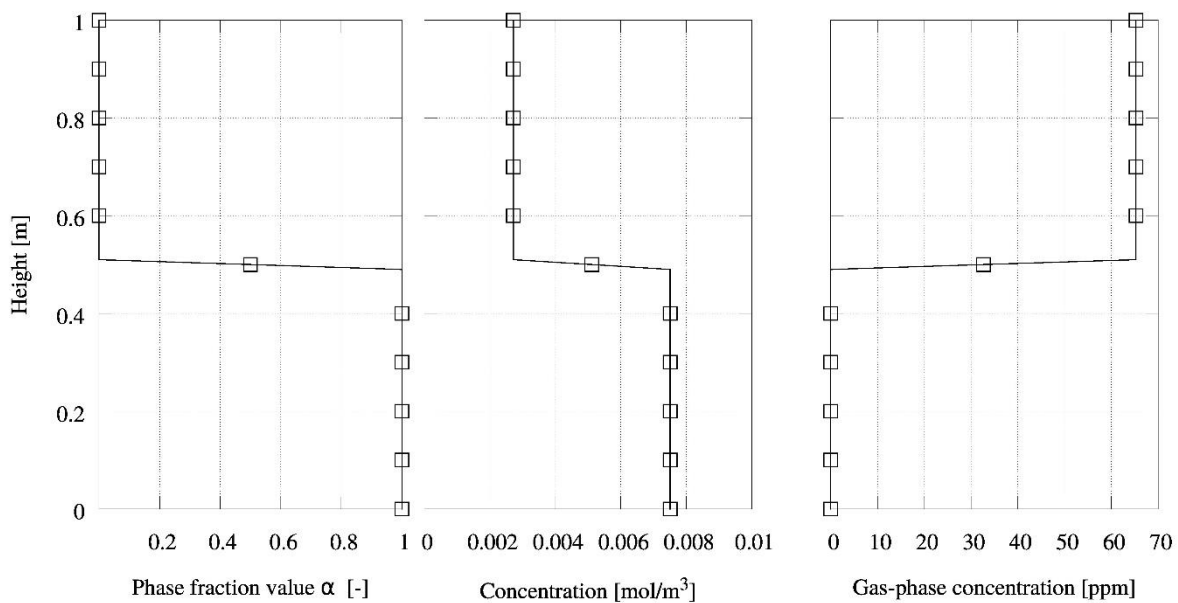
335 *Equilibrium conditions and unit conversion*

336 In order to validate the solver extensions regarding the equilibrium conditions and the partial
 337 pressure in the air phase, example 4.3 by Hvitved-Jacobsen et al. (2013) is simulated. The
 338 resulting H_2S_{aq} and H_2S_g concentrations for a measured concentration of dissolved sulphide c_s
 339 and pH value have been simulated. Again, the basic setup of the case is the same as for the first

340 application example. A temperature of 15°C, $p_{Ka1} = 7.0$, $pH = 7.0$ and a dissolved sulphide
 341 concentration of 0.001 kg/m³ are given.

342 In Hvitved-Jacobsen et al. (2013), the Henry coefficient for the given temperature of 15°C is
 343 assumed to be the same as the Henry coefficient from a previous calculation for a temperature
 344 of 20°C, i.e. 433 atm. For comparing the analytical solution with the simulated values, the exact
 345 Henry coefficient for 15°C has been calculated. Using this value and performing the same
 346 calculation steps with the corrected Henry coefficient, the analytical solution leads to a water
 347 phase H₂S concentration of $c_{H_2S_{aq}} = 0.0075 \text{ mol/m}^3$, a gas phase concentration of $c_{H_2S_g} =$
 348 0.0027 mol/m^3 and a corresponding partial pressure of $p_{H_2S_g} = 66 \text{ ppm}$.

349 Figure 3 shows the results of the numerical simulations. In the water phase, the concentration
 350 of H₂S is $c_{H_2S_g} = 0.0075 \text{ mol/m}^3$, in the air phase the concentration reaches a value of $c_{H_2S_{aq}} =$
 351 0.0027 mol/m^3 and a corresponding partial pressure (in the gas phase) of $p_{H_2S_g} = 66 \text{ ppm}$ and
 352 thus agrees well with the analytical solution. The implemented approach predicts the resulting
 353 concentrations accurately.



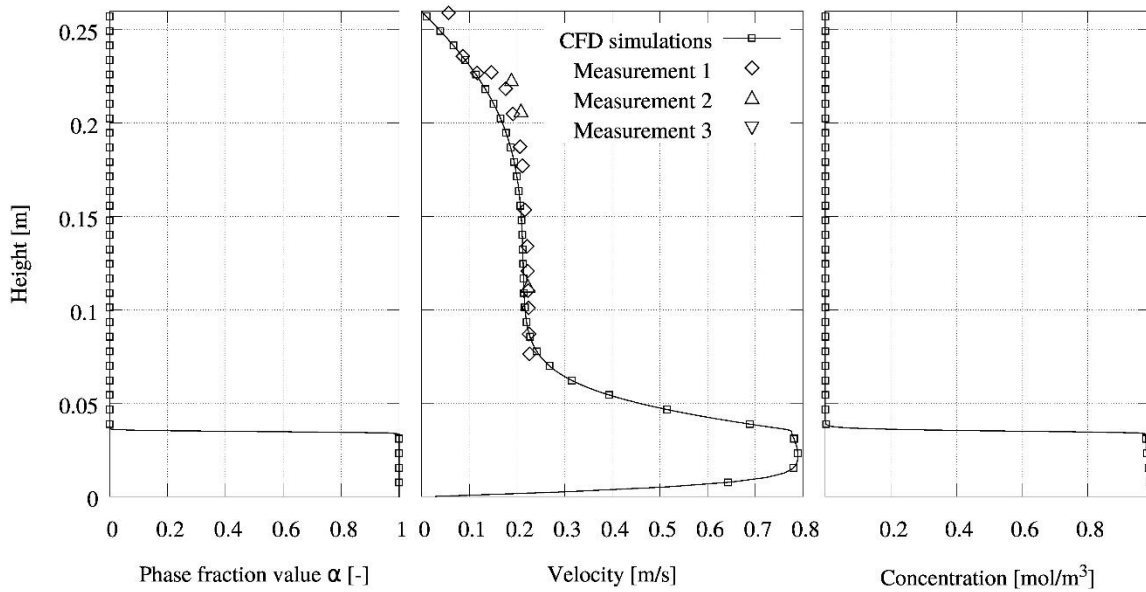
354
 355 *Figure 3. Application example for HS⁻ and H₂S equilibrium and partial pressure of air phase concentration (left: Phase fraction*
 356 *value profile over domain height, middle: concentration profile in, right: partial pressure of gas-phase concentration).*

357

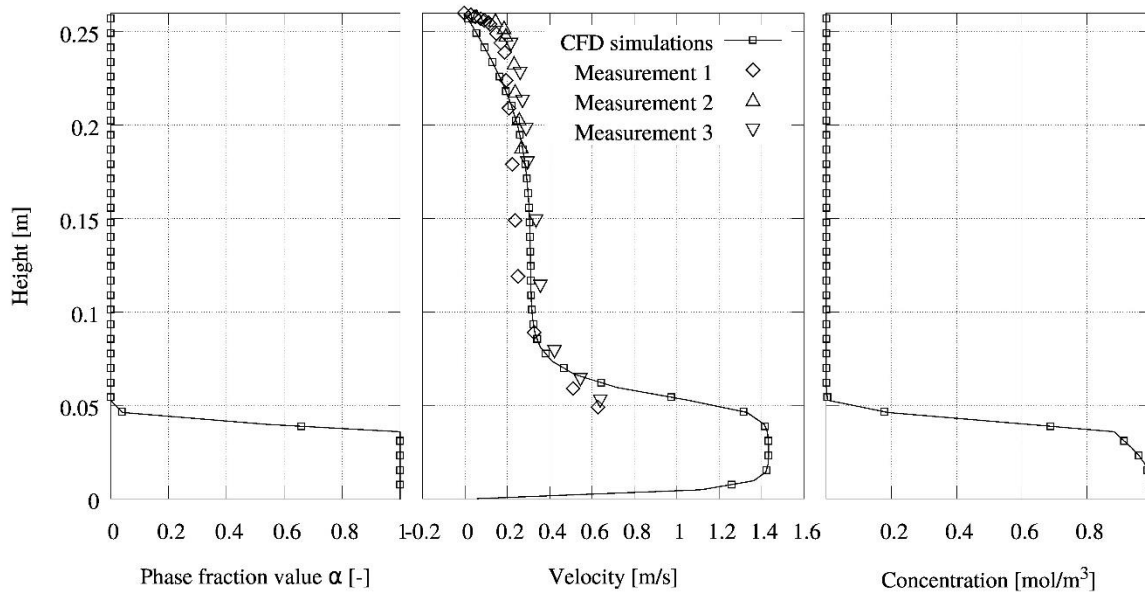
358

359 **Mass transfer in a rectangular channel**

360 In this test case, we present mass transfer simulations in a rectangular pipe. Figures 4 and 5
361 present the resulting phase fraction, velocity and concentration profiles along the height of the
362 domain in the middle of the pipe. The simulated velocity profiles indicate a good agreement
363 with the measured values by Bentzen et al. (2016). For a pipe with a length of 15 m and the
364 analysed flow velocities, the concentration profiles show that almost no mass transfer across
365 the water surface into the air phase can be observed. This can be explained by small velocities
366 in directions other than the main flow direction (i.e. in the yz-plane) which cause advective
367 transport to occur mostly in the main flow direction (x-direction). Furthermore, the small
368 diffusion coefficients cause mainly advective transport. This example opens the question how
369 simulated mass transfer is influenced under highly turbulent conditions or in cases with higher
370 velocities in the yz-plane, which will be analysed in the next example.



372 *Figure 4. Mass transfer in rectangular channel for test 7 (see Table 1) (left: phase fraction value, middle: velocity, right:*
373 *concentration profiles).*



374

375
376

Figure 5. Mass transfer in rectangular channel for test 21 (see Table 1) (left: phase fraction value, middle: velocity, right: concentration profiles).

377 **Complex sewer geometry**

378 In a final example, the advantage of the new model are demonstrated by applying the solver to
 379 a complex and highly three-dimensional sewer geometry. The existing models are not public
 380 domain, therefore a direct comparison to the one-dimensional models is not possible, but the
 381 results of the CFD model will be used to highlight the advantages compared to the concepts of
 382 the existing approaches.

383 The results of the simulations at $t = 10$ s are displayed in Figure 6. Figure 6a) gives an overview
 384 of the computational domain and the water phase behaviour. The location of highest turbulence
 385 occurs in the hydraulic jump, which is displayed in Figures 6b) and 6c). The velocity vectors in
 386 Figure 6b) indicate the highly three-dimensional flow behaviour in this location and show the
 387 complex water surface movement. In Figures 6c) and 6d), the isosurfaces of the resulting H_2S
 388 concentration in the domain are displayed. The concentration range between 0 mol/m^3 and
 389 1 mol/m^3 has been divided into 10 surfaces. The value range in between is not displayed, leaving
 390 white spaces for better illustration of the surfaces. The contour plots show, that a more diverse
 391 and highly three-dimensional concentration profile develops at the reach of the hydraulic jump.
 392 This indicates the increased mass transfer (i.e. higher distance of concentration isolines to the
 393 water surface) in the location of the hydraulic jump.

394 Because the existing model approaches are not public domain, a direct comparison to simulation
 395 results is not possible, however, the advantages of the new CFD based mass transfer approach
 396 are the following:

- 397 (i) In respect to the hydrodynamic behaviour, the new model can describe the three-
 398 dimensional flow velocities in the air and water phase. The sewer geometry analysed
 399 consists of a bent pipe structure with varying shapes and a hydraulic jump. A
 400 hydrodynamic one-dimensional approach would describe this geometry as one
 401 connection pipe between beginning and end point. The flow velocity would be

402 calculated as a uniform value without accounting for the complexity of the
403 geometry. The existing model would not account for the highly complex interaction
404 of water and air phase in the hydraulic jump.

405 (ii) Regarding the mass transfer, the model would then account for advection and
406 molecular diffusion and for turbulence in the free-stream flow areas as well as in
407 drop structures in a very simplified way. This would lead to a simplified assumption
408 of the actual mass transfer occurring in the pipe, since the effect of turbulence on
409 the mass transfer is substantial. A validation of the actual mass transfer rate due to
410 turbulence effects is performed in Teuber et al. (under review).

411 Most sewer stretches in urban areas are not as complex as the previously shown example and
412 wide networks without high levels of turbulence justify the use of one-dimensional models.
413 However, locations of high turbulence can enhance H₂S emissions and the three-dimensional
414 approach presented in this paper can help analyse the effect of local design aspects on the
415 resulting H₂S emissions and improve the sewer network design.

416

417

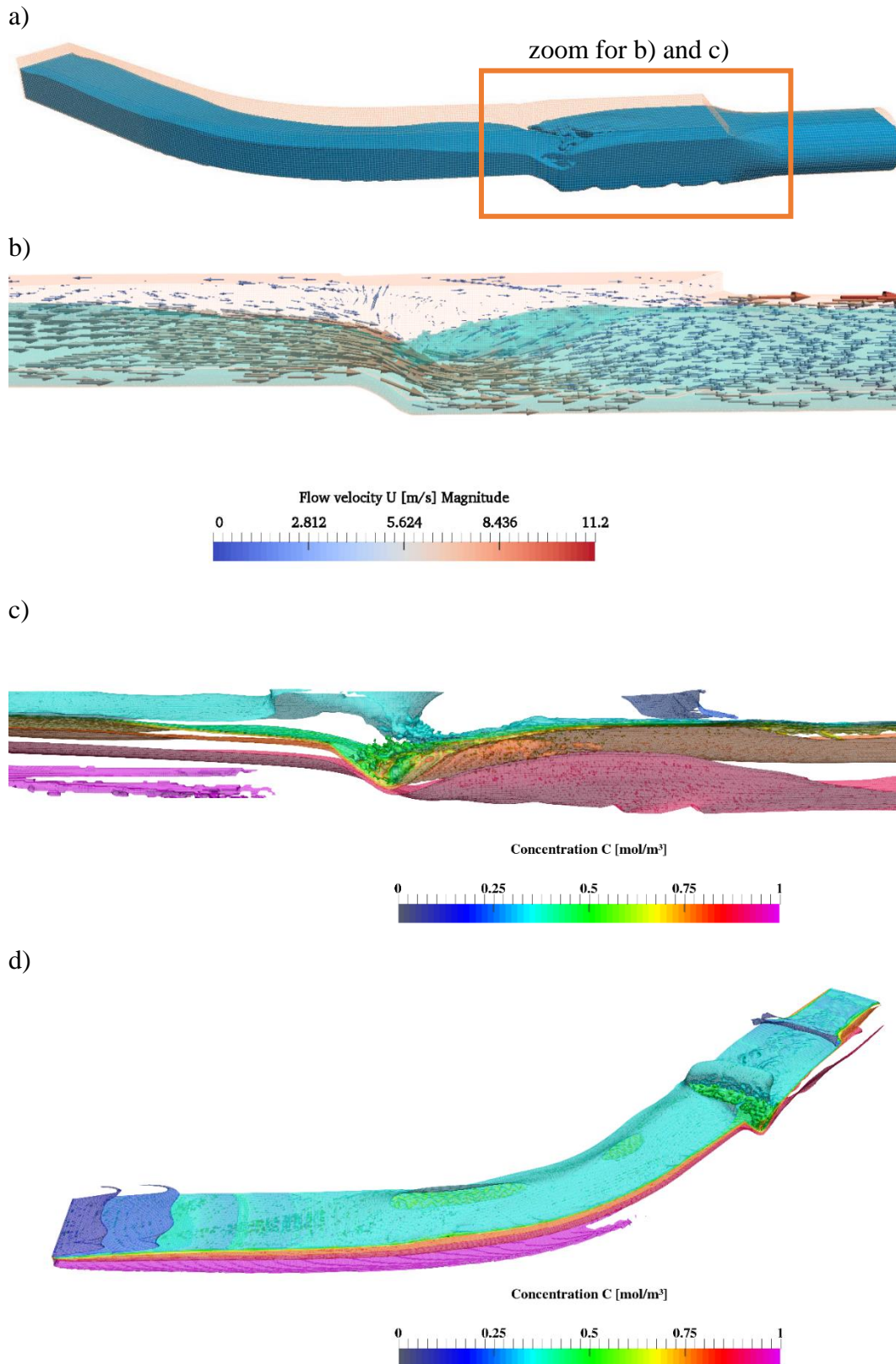


Figure 6. Mass transfer simulations in complex sewer geometry at $t=10s$ (a) overview of the domain filled with water under steady-state conditions, b) flow velocities and water surface behaviour in hydraulic jump, c) top view on tracer distribution, d) tracer distribution in hydraulic jump).

418 Conclusions

419 H₂S emissions and their consequences are an important topic when considering urban drainage
420 and the design of sewer networks. In the past, different model approaches, from empirical to
421 conceptual, have been developed in order to describe and predict H₂S emissions and resulting
422 odour. These models are horizontal one-dimensional, therefore neglecting the occurrence of
423 three-dimensional effects.

424 In this publication, a model approach has been introduced that can describe H₂S emissions
425 across the water surface using a mass transfer approach based on the Henry coefficient, which
426 is implemented in the open source software OpenFOAM. Two-phase flow has been simulated
427 using a VOF method. The solver has been extended by different key features that are crucial
428 when describing H₂S emissions. The temperature dependency of the Henry coefficient has been
429 taken into account. Equilibrium conditions between HS⁻ and H₂S are described and enable the
430 usage of the measured value for total dissolved sulphide and the pH value as input parameters.
431 The solver also computes the partial pressure of H₂S in the gas phase based on the simulated
432 concentration of H₂S_g.

433 The new solver has been applied to different simple test cases and the results have been
434 compared to analytical solutions. Furthermore, it has been applied to a highly complex three-
435 dimensional test case to highlight the advantages of the new model approach. Compared to one-
436 dimensional formulations, it can account for highly complex flow effects in a sewer stretch and
437 describe mass transfer in such environments. The analysis of the results showed an increased
438 mass transfer in the location of highest turbulence, which agrees with existing observations.
439 The exact quantification of local mass transfer rates has been validated in Teuber et al. (under
440 review) and has led to a good agreement with experimental results.

441 Overall, the new solver enables an analysis of mass transfer in complex three-dimensional test
442 cases, the description of which has so far only been possible with major simplifications.

443 Future research will deal with further extensions of the solver to account for temperature effects
444 in the fluids and reactive transport modelling.

445 Acknowledgements

446 The complex sewer geometry has been computed on the supercomputers of Norddeutscher
447 Verbund für Hoch- und Höchstleistungsrechnen in Berlin.

448 The funding provided by the German Research Foundation (DFG) within the Research Training
449 Group ‘Urban Water Interfaces’ (GRK 2032-1) is gratefully acknowledged.

450 We thank Prof. Arnau Bayón for providing the experimental data and the mesh for the complex
451 sewer geometry.

452 References

- 453 Bayón, A., Vallés-Morán, F. J. & López-Jiménez, P. A. 2015 Numerical analysis and validation
454 of South Valencia sewage collection system diversion. In: *36th IAHR World Congress*, The
455 Hague, Netherlands.
- 456 Bentzen, T. R., Østertoft, K. K., Vollertsen, J., Fuglsang, E. D. & Nielsen, A. H. 2016 Airflow
457 in Gravity Sewers - Determination of Wastewater Drag Coefficient. *Water Environment*
458 *Research*, **88**(3), 239-256.
- 459 Carrera, L., Springer, F., Lipeme-Kouyi, G. & Buffiere, P. 2017 Sulfide emissions in sewer
460 networks: focus on liquid to gas mass transfer coefficient. *Water Science and Technology*,
461 **75**(8), 1899-1908.
- 462 Edwini-Bonsu, S. & Steffler, P. M. 2006 Dynamics of air flow in sewer conduit headspace.
463 *Journal of Hydraulic Engineering*, **132**(8), 791-799.
- 464 Gilchrist, F.M.C. 1953. Microbiological studies of the corrosion of concrete sewers by
465 sulphuric acid producing bacteria. *South African Journal of Chemistry*, 214–215.
- 466 Haroun, Y., Legendre, D. & Raynal, L. 2010 Volume of fluid method for interfacial reactive
467 mass transfer: application to stable liquid film. *Chemical Engineering Science*, **65**(10), 2896-
468 2909.
- 469 Haroun, Y., Legendre, D. & Raynal, L. 2010 Direct numerical simulation of reactive
470 absorption in gas-liquid flow on structured packing using interface capturing method.
471 *Chemical Engineering Science*, **65**(1), 351-356.
- 472 Hvitved-Jacobsen, T., Vollertsen, J. & Nielsen, A.H. 2013 Sewer processes: microbial and
473 chemical process engineering of sewer networks, 2nd edn., *CRC press*.
- 474 Matias, N., Nielsen, A. H., Vollertsen, J., Ferreira, F. & Matos, J. S. 2017 Erratum: Water
475 Science and Technology 75 (10), 2257–2267: Liquid-gas mass transfer at drop structures. *Water*
476 *Science and Technology*, **76**(6), 1584-1594.
- 477 Matias, N., Nielsen, A.H., Vollertsen, J., Ferreira, F. & Matos, J. S. 2017 Liquid-gas mass
478 transfer at drop structures. *Water Science and Technology*, **75**(10), 2257–2267.
- 479 Nieves-Remacha, M.J., Yang, L. & Jensen, K.F. 2015 OpenFOAM computational fluid
480 dynamic simulations of two-phase flow and mass transfer in an Advanced-Flow Reactor.
481 *Industrial & Engineering Chemistry Research*, **54**(26), 6649-6659.
- 482 Rootsey, R. & Yuan, Z. 2010 New insights into sewer odour and corrosion. In: *6th International*
483 *Conference on Sewer Processes and Networks*, Queensland, Australia.
- 484 Rootsey, R., Melchers, R., Stuetz, R., Keller, J. & Yuan, Z. 2012 Taking control of odours and
485 corrosion in sewers. In: *Australia's National Water Conference and Exhibition (OzWater*
486 *2012)*, Sydney, Australia.
- 487 Rusche, H. 2003 *Computational fluid dynamics of dispersed two-phase flows at high phase*
488 *fractions*, PhD thesis, Imperial College London (University of London), London, United
489 Kingdom.

- 490 Sander, R. 2015 Compilation of Henry's law constants (version 4.0) for water as solvent.
491 *Atmospheric Chemistry and Physics*, **15**, 4399-4981.
- 492 Severin, T. S. 2017 *Computational Fluid Dynamics Assisted Design of Thin-Layer Cascade*
493 *Photobioreactor Components*, PhD thesis, Technische Universität München, Munich,
494 Germany.
- 495 Teuber, K., Broecker, T., Bayón, A., Nützmann, G. & Hinkelmann, R. (in press) CFD-
496 modelling of free-surface flows in closed conduits. *Progress in Computational Fluid Dynamics*.
- 497 Teuber, K., Broecker, T., Nützmann, G. & Hinkelmann, R. (under review) CFD simulation of
498 H₂S mass transfer under turbulent conditions in a stirring tank, *submitted to Water Science*
499 *and Technology on April 12, 2019*.
- 500
501 Thistlethwayte, D. K. B. 1972 Control of sulphides in sewerage systems. *Ann Arbor Science*.
- 502 Thorenz, C. & Strybny, J. 2012 On the numerical modelling of filling-emptying systems for
503 locks. In: *Proceedings of the 10th International Conference on Hydroinformatics (HIC)*,
504 Hamburg, Germany.
- 505 Wang, C., Xu, Z., Lai, C. & Sun, X. 2018 Beyond the standard two-film theory: Computational
506 fluid dynamics simulations for carbon dioxide capture in a wetted wall column. *Chemical*
507 *Engineering Science*, **184**, 103–110.
- 508 Yang, L., Nieves-Remacha, M. J. & Jensen, K. F. 2017 Simulations and analysis of multiphase
509 transport and reaction in segmented flow microreactors. *Chemical Engineering Science*, **169**,
510 106-116.
- 511 Yongsiri, C., Vollertsen, J. & Hvitved-Jacobsen, T. 2004 Effect of temperature on air-water
512 transfer of hydrogen sulfide. *Journal of Environmental Engineering*, **130**(1), 104-109.
- 513